Energy Technology Division
Energy Technology Division
Energy Technology Division
Energy Technology Division
Energy Technology Division
Energy Technology Division
Energy Technology Division
Energy Technology Division
Energy Technology Division
Energy Technology Division
Energy Technology Division
Energy Technology Division
Energy Technology Division
Energy Technology Division
Energy Technology Division
Energy Technology Division
Energy Technology Division
Energy Technology Division
Energy Technology Division
Energy Technology Division
Energy Technology Division
Energy Technology Division
Energy Technology Division
Energy Technology Division
Energy Technology Division
Energy Technology Division
Energy Technology Division
Energy Technology Division
Energy Technology Division
Energy Technology Division
Energy Technology Division
Energy Technology Division
Energy Technology Division
Energy Technology Division

ANL-00/1

Modeling of MHD Edge Containment in Strip Casting with ELEKTRA and CaPS-EM Codes

(Including User Guide for Modeling of MHD Edge Containment in Strip Casting)

by F. C. Chang

Argonne National Laboratory, Argonne, Illinois 60439
operated by The University of Chicago
for the United States Department of Energy under Contract W-31-109-Eng-38

Energy Technology Division
Energy Technology Division
Energy Technology Division
Energy Technology Division
Energy Technology Division
Energy Technology Division
Energy Technology Division
Energy Technology Division

Argonne National Laboratory, with facilities in the states of Illinois and Idaho, is owned by the United States government, and operated by The University of Chicago under the provisions of a contract with the Department of Energy.

Reproduced from the best available copy.

Available to DOE and DOE contractors from the
Office of Scientific and Technical Information
P.O. Box 62
Oak Ridge, TN 37831
Prices available from (423) 576-8401

Available to the public from the
National Technical Information Service
U.S. Department of Commerce
5285 Port Royal Road
Springfield, VA 22161

ARGONNE NATIONAL LABORATORY
9700 South Cass Avenue, Argonne, Illinois 60439

ANL-00/1

Modeling of MHD Edge Containment in Strip Casting with ELEKTRA and CaPS-EM Codes

(Including User Guide for modeling of MHD Edge Containment in Strip Casting)

by
F. C. Chang
Energy Technology Division

January 2000

Work sponsored by
U.S. DEPARTMENT OF ENERGY
Office of Energy Research
Laboratory Technology Transfer Program

Contents

Figures

Tables

Modeling of MHD Edge Containment in Strip Casting with ELEKTRA and CaPS-EM Codes

Fon-Chieh Chang
Argonne National Laboratory

Abstract

This paper presents modeling studies of magnetohydrodynamics analysis in twin-roll casting. Argonne National Laboratory (ANL) and ISPAT Inland Inc. (Inland), formely Inland Steel Co., have worked together to develop a three-dimensional (3-D) computer model that can predict eddy currents, fluid flows, and liquid metal containment of an electromagnetic (EM) edge containment device. The model was verified by comparing predictions with experimental results of liquid metal containment and fluid flow in EM edge dams (EMDs) that were designed at Inland for twin-roll casting. This mathematical model can significantly shorten casting research on the use of EM fields for liquid metal containment and control. The model can optimize the EMD design so it is suitable for application, and minimize expensive time-consuming full-scale testing.

Numerical simulation was performed by coupling a 3-D finite-element EM code (ELEKTRA) and a 3-D finite-difference fluids code (CaPS-EM) to solve heat transfer, fluid flow, and turbulence transport in a casting process that involves EM fields. ELEKTRA can predict the eddy-current distribution and the EM forces in complex geometries. CaPS-EM can model fluid flows with free surfaces. The computed 3-D magnetic fields and induced eddy currents in ELEKTRA are used as input to temperature- and flow-field computations in CaPS-EM. Results of the numerical simulation compared well with measurements obtained from both static and dynamic tests.

1 Introduction

Steel sheets, which are widely used in the automotive and appliance industries, are now made mainly by continuous casting of 50- to 300-mm-thick slabs, followed by hot rolling to reduce the thickness to ≈ 2.5 mm, and then by cold rolling to the final thickness. A schematic representation of traditional slab casting is shown in Fig. 1. Because hot-rolling stage is very capital- and energy-intensive, it adds significantly to the cost of the finished product. The need of industry to develop its capability to cast relatively thin sheets of steel is urgent. If thin sheets could be cast, the entire hot-rolling portion of the process could be eliminated. The cost savings would give the sheet product an enormous economic advantage over products made by competing methods.

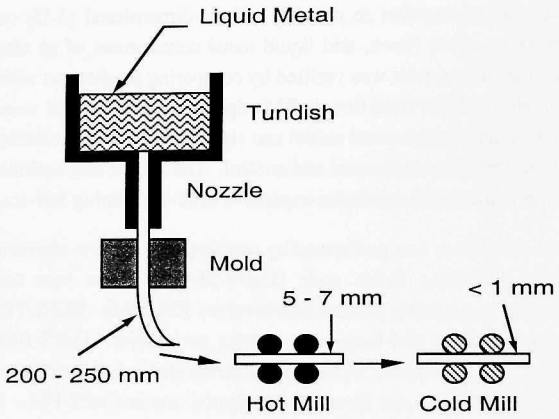

Fig. 1. Schematic representation of conventional slab casting

Twin-roll casting has been used to produce wide, thin aluminum strips. Several twin-roll processes are used to cast strips that are 2 to 5 mm thick and 1500 to 2000 mm wide [1-5]. Traditionally, this technique for casting thin strips requires some type of ceramic material at the ends of counter-rotating rollers to contain the molten metal pool, as shown in Fig. 2. Ceramic dams endure for only a short time and are susceptible to erosion and breakage. They also are sites on which the molten metal can solidify, and this solidified metal can become attached to the strip that is being formed and thus alter the roll gap spacing, and hence the thickness of the cast product and its surface temperature. These alternations can lead to surface defects, variation in product thickness, leakage of liquid steel from the caster, and even strand breakage and liquid steel breakouts.

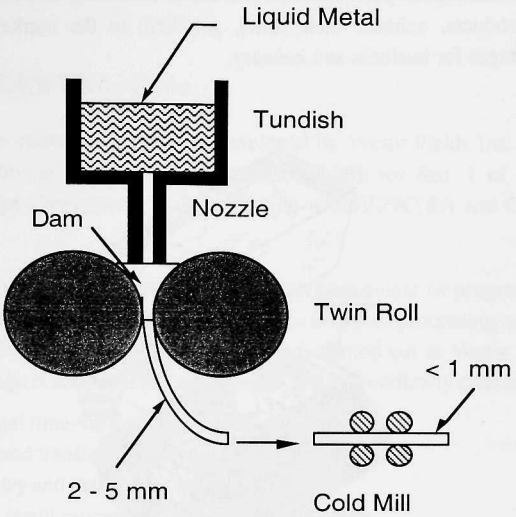

Fig. 2. Schematic representation of twin-roll casting with ceramic solid dam

Magnetics is increasingly being used in a broad range of metallurgical applications, from relatively mature applications, such as the electromagnetic (EM) mold for casting aluminum [6]; to emerging or proposed applications, such as levitation and/or confinement in the entry region between the tundish and a horizontal casting mold, edge confinement [7] and control [8] within a strip or plate caster, and control of shape (e.g., thickness); to nearly final form specifications [9]. In virtually all such applications, an alternating EM field is used to induce current to flow within the molten metal to create the desired confinement forces. The confinement forces work against a static head that, in many applications, is primarily gravitational.

Use of the EM field will play a major role in the evolution of the steel industry [10-14] because under these circumstances, no contact is made with the steel, defects can be minimized, and product quality can be improved. Many problems with product quality are related to mold and air-gap formation, and to interaction between the ingot shell and the liquid core. Moldless casting, wherein an EM field supports the liquid metal until it enters the direct-quench zone, could eliminate these problems. The application of EM edge dams (EMDs) in twin-roll casting (Fig. 3) can bypass the fundamental problems of ceramic solid dams and make economic sense [15,16]. In other words, if the EMD concept is successful, all of the problems associated with ceramic edge containment could be eliminated and the possibility of successfully developing a twin-roll strip casting process for steel would be significantly increased. Application of EM fields in twin-roll casting is a complicated process that involves interaction among electric, magnetic, thermal,

mechanical, and metallurgical phenomena. Therefore, modeling is needed to help optimize the performance of products, enhance their value, get them to the marketplace sooner, and gain competitive advantages for business and industry.

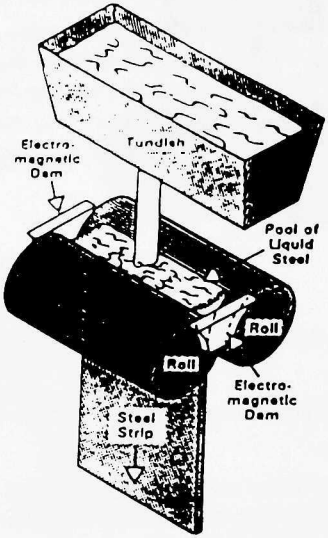

Fig. 3. Twin-roll casting with EMDs

Argonne National Laboratory (ANL) and Inland have worked together to develop a 3-D computer model that can predict fluid flows and eddy currents in EMDs for twin-roll casting. Numerical simulations were performed to compute the EM force and fluid flow by coupling the finite-element EM code ELEKTRA and the finite-difference casting process magnetohydrodynamic (MHD) code CaPS-EM. ELEKTRA solves 3-D time-varying EM field equations and predicts the induced eddy currents and EM forces. The time variation can be either transient or steady-state AC. CaPS-EM provides an efficient solution for transient heat conduction within the metal and between the metal and the mold and computes the profile of the free surface [17]. The computed 3-D magnetic fields and induced current densities in ELEKTRA are used as input for flow-field computations in CaPS-EM. The model developed by ANL and Inland involves solution of the Maxwell equations, the Navier-Stokes equations, and the transport equations for turbulence kinetic energy k and its rate of dissipation ε. Turbulent flow is included to describe recirculating, electromagnetically induced flows, and control of turbulent flow in the liquid metal is an efficient way to improve performance of the EM system. The model utilizes the design data and operating

parameters of both static and dynamic test rigs of an industrial twin-roll caster to compute transient fluid flows.

2 Synopsis of ELEKTRA Code

The ELEKTRA is commercial software developed by Vector Fields Inc. in England for 3-D eddy current computation and electromagnetic design [18-20]; see Sec. 1 of the User Guide for Modeling of MHD Edge Containment in Strip Casting with ELEKTRA and CaPS-EM codes (the Appendix).

The ELEKTRA package is a sound-generation-integrated suite of programs for 3-D analysis of eddy currents. The package includes powerful pre- and post-processing modules linked to an analysis module of advanced design, based on research carried out at Vector Fields and Philips, Eindhoven. The package is used in many applications and is specifically characterized by:

- three-dimensional time-varying EM fields,
- time harmonic and transient fields, motional effects,
- efficient geometry and data input facilities, and
- comprehensive result processing and 3-D model display.

ELEKTRA uses a discrete finite-element model to solve the partial differential equations that govern the behavior of a system and includes the EM finite-element pre- and post-processor OPERA-3D.

2.1 Model Generation

Using OPERA a mesh is formed which is automatically subdivided into elements. A 2-D grid is created initially and is swept through space to create a 3-D model. The sweep operation includes facilities for rotation, projection, and translation. The resulting model has the following features: -

- 3-D curved surfaces,
- tetrahedral, prism, and brick primitives,
- conductors modeled separately,
- wire frame and hidden surface displays, and
- light-source shading option for display purposes.

The mesh primitive blocks are assigned orientation and material characteristics. The resultant input is fed directly into the analysis module.

2.2 Analysis

ELEKTRA solves the 3-D time-varying magnetic field equations. The time variation can either be transient or alternating (steady state). In addition, the effects due to motion can be computed. Total and reduced magnetic scalar potentials are used in non-conducting media. Use of

these scalar potentials reduces the solution costs and corrects the cancellation errors associated with the simple reduced-potential approach. In conducting media, the program uses the magnetic vector and electric scalar potentials, which are directly coupled with the potentials on the exterior. The use of magnetic vector and electric scalar potentials now enables accurate modeling of both DC solutions and different conductors in contact.

2.3 Post-Processing

OPERA provides the user facilities to display the results of the analysis in several ways, including

- 3-D model views from any angle,
- graphs, histograms, and contour maps of the solutions,
- contours of components of the results on any surface,
- calculation of fields, forces, and energy,
- particle tracking, and
- user-defined function.

3 Synopsis of CaPS-EM Code

Argonne National Laboratory and Inland have worked together under a Cooperative Research and Development Agreement (CRADA) to modify ANL software that could help steel companies model continuous casting at substantial savings of production cost and energy. This joint effort has provided a 3-D computer model, the macroscopic casting process simulator with EMs (CaPS-EM), that can predict fluid flows and eddy currents in molten steel. The model CaPS-EM is verified by predicting liquid metal containment and fluid flow in caster designs for application at a demonstration plant.

Previous research involved the use of magnetic fields to contain liquid metal in an experimental thin-strip caster [16]. The research involved expensive bench-scale testing devices that cast molten metals but did not simulate large-scale industrial casters. However, it was necessary to follow bench-scale testing in a pilot-scale caster.

The CaPS-EM significantly shorten casting research that involves the use of EM fields for liquid metal containment, stirring, and control. The model also optimizes the existing casting processes and minimizes expensive, time-consuming, full-scale testing. The cost savings from thin-strip casting would give the sheet product an enormous economic advantage over competing methods. Thin-strip casting has the potential to achieve this technological breakthrough, giving the U.S. steel industry a strong competitive edge over its foreign competitors. Steel sheet is used extensively in the automotive and appliance industries, which stand to gain from the successful development of this process.

The above-described work was supported by the Department of Energy (DOE), Office of the Energy Research, Laboratory Technology Transfer Program. Argonne's work under this CRADA is an extension of past DOE work on EM casting and on the Casting Process Simulation (CaPS) code, which was supported by DOE's Office of Conservation and Renewable Energy. Other research and development on which the work is based includes eddy-current modeling work supported by DOE's Fusion Power Program.

3.1 Features of CaPS-EM Code

The CaPS-EM software combines heat transfer, fluid flow, and EM-field aspects, and can describe various solidification aspects, including mold filling and containment. CaPS-EM is a 3-D time-dependent computer code that involves a finite-volume formulation for the mass, momentum, energy, and turbulent-flow equations; its origin is in CaPS [17] and it exhibits the following characteristics:

- CaPS-EM uses the Casting Pre-processor (CPRE) geometric modeling package to construct the geometry, generate a neutral file that consists of a list of named components, and post-process the simulation results; it builds the geometry independently of the mesh, a time-saving procedure. Each named component involves a set of hyperpatches, patches, or grids that are included in the session file to create the geometry.

- A mesh generator of structured regular cells is included and is interfaced with the neutral-file output of the solid geometric package.

- Visual user interfaces that are based on the HOOPS package, which contains a hierarchical database of geometric information, have been developed. These visual interfaces allow the user to observe, create, verify, and view the meshed geometry, set up the boundary and initial conditions, view the various named components, and initialize the simulation parameters (e.g., maximum time allowed for the run, iteration time interval, maximum number of steps, step interval for graphical output, etc.).

- The CaPS-EM generates a data file to read EM-field data from ELEKTRA into CaPS-EM.

- The CaPS-EM shell scripts interactively provide a step-by-step procedure to simulate the solidification process, thus making the software very user friendly.

CaPS-EM efficiently solves transient heat conduction within the metal and between the metal and the mold and should be used in conjunction with CPRE and HOOPS packages. With CaPS-EM, containment techniques can be improved by validating the design of the edge dam system to increase both magnetic field and magnetic force. Also, optimization can be achieved by computing

the effects of key parameters in the process. CaPS-EM is an efficient software tool that saves time and energy and reduces surfacing work while producing more efficient casting of thin slabs.

3.2 Organization of CaPS-EM Model

An overview of CaPS-EM is provided to give the user a feeling for what the CaPS software requires and what it can do. A flow chart is provided in Section 3.4 of this report to show the various modules of CaPS-EM and their contributions to the simulation.

The first step in modeling with CaPS-EM software is to build the geometry. CaPS-EM interacts with CPRE via the neutral file. The step after building the geometry is to either divide the geometry into rectangular cells (meshing) or set the boundary and initial conditions so the various configurations are similar to those used in real procedures. Once the geometry is set and the boundary and initial conditions are assigned to various parts of the geometry, geometric meshing can be performed.

The input file to begin the simulation is described in Sec. 2.1 of the Appendix. Section 2.2 of the Appendix describes how hard-copy output can be obtained for various parameters with the Print Step feature of CaPS-EM. In CaPS-EM, material properties are temperature-dependent and are to be included in the properties database directory.

As mentioned earlier, CaPS-EM software originated from the CaPS code and is extended to MHD application by accounting for the EM-field effect. Therefore, more information and guidelines are listed in the "User Guide for the Casting Process Simulator Software CaPS-2D" [17].

3.3 Overview of CaPS-EM Modules

Several modules of CaPS-EM can be used to facilitate the geometric setup and to submit a simulation run. The CaPS-EM shell scripts perform all of the linkages, and the user generally need not worry about file structure.

The CaPS-EM shell scripts make up an important user-friendly tool that links all files and directories and thus does not burden the user with creating links, etc. The visual interfaces (Vbounds and Vmesher) facilitate the setup of initial and boundary conditions and geometry meshing. Post-processing can be performed either with the Print Step load module that provides hard-copy output of the variables for particular time steps, or with Casting Post-processor (CPOST), which is linked to the Cas load module via Capspat. Thus, the simulation results can be displayed in CPOST, and the various plots of velocity vectors, solid mass fraction, temperature isotherms, and fluid volume can be analyzed to understand fluid flow and heat transfer for the part assembly in the geometry.

Next, we will discuss how various input and output files are linked and placed in the working directory. CaPS-EM creates the files according to the working modules and links or copies the various files in the current working module. In this way, the time lost in input/output processes is minimized.

3.4 Flow Chart of CaPS-EM Software

Figure 4 shows the flow chart of the CaPS-EM software and indicates the modules that must be set and initialized before going to the next module down the flow chart. Initially, the geometry is set up with the CPRE software.

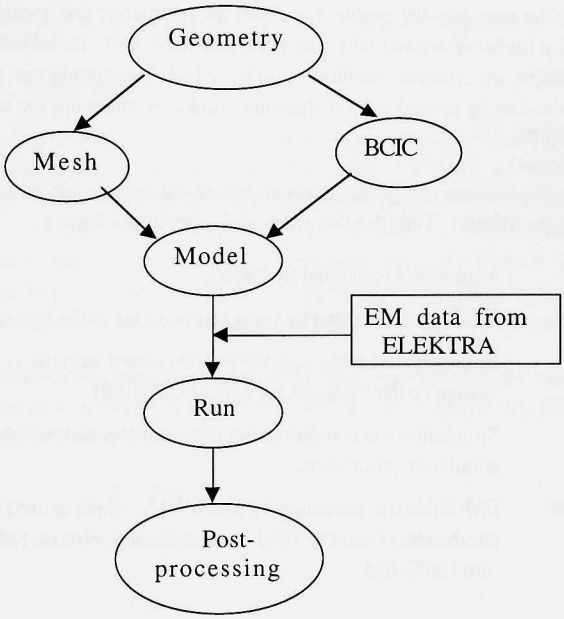

Fig. 4. Flow chart of CaPS-EM software

The geometry is built by using grids, patches, and hyperpatches. Patches and hyperpatches are grouped into user-defined, named components to facilitate boundary condition and initial condition (BCIC) assignments, respectively. These named components are the basis upon which the boundary conditions identify various sections of the geometry. Next, a neutral file is created.

Because this neutral file contains the descriptions of the named components, it is a link that enables CaPS-EM to compute the geometric hyperpatch volumes, display the geometry in the visual interfaces, and identify the various geometric sections.

The meshing of the geometry and the setup of the initial and boundary conditions are on the same level and thus either module can be initiated. The geometric volumes created with CPRE can be initialized and the surfaces can be assigned specific boundary conditions with the Vbound module. The meshing is performed by the visual Vmesher interface. These visual interfaces can easily detect any geometric flaws. If flaws are detected, the user must start again by creating or rectifying the geometry with CPRE and then, after computing the hyperpatch volumes, the Vbounds and Vmesher can again be initiated.

After the user sets the problem, meshes the geometry, and applies the boundary and initial conditions, a model is created with one particular mesh and one particular set of conditions. The model contains the various conditions under which the simulation runs are to be conducted. Multiple runs can be carried out for the same model by changing the conditions of the simulation via the *.TS file.

Once the runs are completed, the post-processing module can be initiated and the simulation results may be viewed. The files that show up in the simulation are

*NE	Neutral file generated by CPRE.
*ME	Meshing file created by using the vi editor or the Vmesher module of CaPS-EM.
*BC	Boundary and initial conditions file created with the vi editor of the Unix system or the Vbounds module of CaPS-EM.
*TS	Simulation run conditions file to be used by CaPS-EM to set the various simulation parameters.
*EMF	EM-fields file generated by ELEKTRA, which is used to input the EM-field parameters (magnetic field, current density, electric field, and magnetic force) into CaPS-EM.

4 Mathematical Model and Numerical Procedure

In this study, numerical simulations were performed to compute the EM force and fluid flow by coupling the finite-element code ELEKTRA and the finite-difference casting process MHD code CaPS-EM. In this EM casting, fluid flow of liquid metal with a free surface under EM force was investigated numerically. The volume fraction method was introduced to treat the free surface, and the magnetic potential was used for eddy-current analysis. The shape of the free surface is governed primarily by the balance of EM pressures against pressures due to gravity. Transfer of momentum due to both flows of molten metal and turbulence may also be critically important.

Quantitative mathematical representation of this system involves the induced current, the EM field, the EM force, and the resultant fluid flow. The resultant model involves solutions of the Maxwell equations, the Navier-Stokes equations, and the transport equations for the turbulence kinetic energy and its rate of dissipation. A turbulent-flow model is included in CaPS-EM to describe recirculating electromagnetically induced flows. Control of turbulent flow in the liquid metal can be an efficient method for improving performance of the EM system. These steps may be conveniently divided into EM calculations and fluid flow computations.

The following assumptions and simplifications are made in the mathematical model:

- All flows are assumed to be isotropic and at steady state.
- Fluid flow due to causes other than EM action (e.g., pouring stream) is not included in the simulation.
- Time-averaged values of the EM forces are appropriate for fluid-flow calculations.

4.1 Electromagnetic Equations

ELEKTRA uses a combination of vector and scalar magnetic potentials to model time-varying EM fields. Vector potentials are used in conducting media, and scalar potentials are used elsewhere. In time-varying fields, the currents induced in conducting volumes are some of the unknowns in the system. Therefore, their fields cannot be evaluated by simply performing an integration. Inside the conducting volumes, the field representation must include a rotational component. ELEKTRA combines the efficient total-and-reduced scalar potential method for non-conducting volumes with an algorithm that uses a vector potential in the conducting volumes.

In a low-frequency time-varying magnetic field, when the dimensions of the objects in the space are small when compared with the wavelengths of the fields, the magnetic and electric fields are related by the low-frequency limit of Maxwell's equations:

Magnetic flux density: $$\bar{\nabla} \bullet \bar{B} = 0 \qquad (1)$$

Ampere's Law: $$\bar{J} = \bar{\nabla} \times \bar{H} \qquad (2)$$

Faraday's Law: $$\bar{\nabla} \times \bar{E} = - \partial \bar{B} / \partial t \qquad (3)$$

and

Ohm's Law: $$\bar{J} = \sigma (\bar{E} + \bar{U} \times \bar{B}), \qquad (4)$$

where σ is the electrical conductivity, $\bar{B}$ is the magnetic flux density, $\bar{E}$ is the electric field strength, $\bar{H}$ is the magnetic field strength, and $\bar{J}$ is the current density. Once the current distribution and the vector potential are known, the magnetic field is readily calculated and one may then obtain the EM force $\bar{F}$ by solving the relationship

$$\bar{F} = \bar{J} \times \bar{B}. \tag{5}$$

4.2 Fluid Flow Equations [Refs. 17, 21]

The conservation equations of continuity, motion, and energy in CaPS-EM are developed by the mass, momentum, and energy balance, respectively, over a control volume, i.e.,

$$\frac{\partial \rho}{\partial t} + \frac{\partial (\rho U_i)}{\partial x_i} = 0. \tag{6}$$

Equation 6 indicates that the rate of mass accumulation is the difference between the rate of mass into and mass out of the control volume, i.e.,

$$\rho \frac{\partial U_i}{\partial t} + \rho U_j \frac{\partial U_i}{\partial x_j} = \frac{\partial}{\partial x_j}\left[(\mu_\ell + \mu_t)\frac{\partial U_i}{\partial x_j}\right] - \frac{\partial p}{\partial x_i} + \rho g_i + \varepsilon_{ijk} J_j B_k. \tag{7}$$

In Eq. 7, the terms on left-hand side indicate the rate of increase of momentum. The terms on the right-hand side are the rate of momentum gain by convection, the pressure force on an element, the rate of momentum gain by viscous transfer, the gravitational force on an element, and the EM force on an element, respectively.

4.3 Energy Transport Equation

Temperature profiles are calculated from electrothermal heating (Joule heating) and an energy balance. Heat is transferred from the roller surfaces to the liquid metal by convection,

$$\rho c_p \frac{\partial T}{\partial x_i} = \frac{\partial}{\partial x_i}\left(k \frac{\partial T}{\partial x_i}\right) + \sigma E_i E_i \tag{8}$$

4.4 Turbulence Model

The k-ε model is used for the bulk of the liquid. The transport equations that describe the time and space distributions of turbulence kinetic energy k and its rate of dissipation ε (Eqs. 9 and 10) are given in terms of production, buoyancy, dissipation, and diffusion. The EM effect on turbulence is implied by the last term of Eq. 9 [22].

$$\rho \frac{\partial k}{\partial t} + \rho U_j \frac{\partial k}{\partial x_j} = P_k + G_k - \rho \varepsilon + \frac{\partial}{\partial x_j}\left[\left(\frac{\mu_t}{\sigma_k} + \mu_\ell\right)\frac{\partial k}{\partial x_j}\right] - \frac{4}{3} c_{MHD} \sigma k B_j B_j \tag{9}$$

$$\rho\frac{\partial \varepsilon}{\partial t}+\rho U_j\frac{\partial \varepsilon}{\partial x_j} = c_{1\varepsilon}\frac{\varepsilon}{k}(P_k+G_k) - c_{2\varepsilon}\rho\frac{\varepsilon^2}{k} + \frac{\partial}{\partial x_j}\left[\left(\frac{\mu_t}{\sigma_\varepsilon}+\mu_\ell\right)\frac{\partial \varepsilon}{\partial x_j}\right]. \tag{10}$$

In Eqs. 9 and 10, P_k and G_k are defined in Ref. 23 as follows:

$$P_k = \mu_{eff}\left[\frac{\partial U_i}{\partial x_j}\left(\frac{\partial U_i}{\partial x_j}+\frac{\partial U_j}{\partial x_i}\right)\right] \tag{11}$$

and

$$G_k = -\frac{\mu_t}{\rho\,\sigma_h}\frac{\partial \rho}{\partial T}\left(\frac{\partial T}{\partial x_j}\,g_j\right). \tag{12}$$

In Eqs. 9-12, P_k is the source term due to mean shear and G_k is the source term due to thermal buoyancy. σ_h (= 0.9) is the turbulence Prandtl number that is used to calculate conductivity, and σ_k (=1.0) is the turbulence Prandtl number for k. σ_ε (=1.3) is the turbulence Prandtl number for ε, $c_{1\varepsilon}$ (=1.44) is the coefficient of turbulence production, and $c_{2\varepsilon}$ (=1.92) is the coefficient for decay-of-grid turbulence. The effective viscosity μ_{eff} (= $\mu_\ell + \mu_t$) is the sum of laminar and turbulent viscosities.

In the immediate vicinity of a solid wall, the values of turbulence properties vary significantly. Therefore, the wall function treatment is applied to predict the correct values of momentum flux, energy flux, and gradients of k and ε. Figure 5 shows the two-layer wall function model [23] used in the simulation. When $y_p > y_\ell$, the first node is in the fully turbulent zone and one has

$$k_p = u^{*2}/\sqrt{c_\mu} \tag{13}$$

and

$$\varepsilon_p = u^{*3}/(K\,y_p). \tag{14}$$

When $y_p \le y_\ell$, the node P is in the laminar sublayer and one has

$$k_p = u^{*2}(y_p/y_\ell)/\sqrt{c_\mu} \tag{15}$$

and

$$\varepsilon_p = u^{*3} / (K\, y_\ell), \tag{16}$$

where the constant $c_\mu = 0.09$, K (= 0.42) is the von Karman constant, and the constant E (= 9.0) is determined from the roughness of the wall.

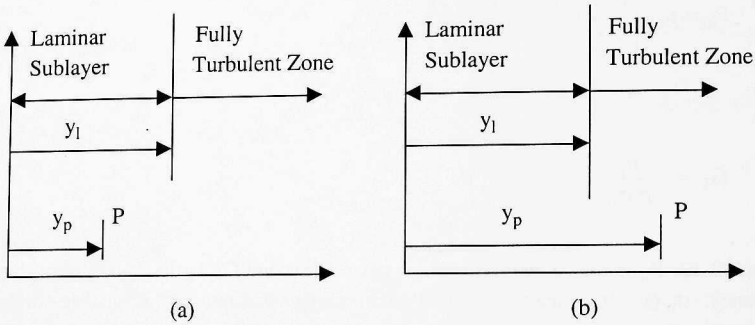

Fig. 5. Schematic representation of two-layer wall function model: (a) $y_p < y_l$ and (b) $y_p > y_l$

4.5 Dynamic Test Rigs

A functional strip caster uses two counter-rotating rollers. The liquid metal is injected from the nozzle and exits from the nip of the rollers. The nozzle is at the center between the two rollers, and is submerged in the liquid (Fig. 3). The shear force F_w is a momentum transport from the rotating rollers to the liquid metal near the rollers. In the numerical model, F_w is treated as an external source in the momentum equations and is applied only to the boundary cells that are next to the rollers.

$$F_{w,x} = A_x\, \tau_{w,x} = A_x\, \mu\, (\partial U/\partial n)_{w,x} \tag{17}$$

$$F_{w,y} = A_y\, \tau_{w,y} = A_y\, \mu\, (\partial U/\partial n)_{w,y} \tag{18}$$

$$F_{w,z} = A_z\, \tau_{w,z} = A_z\, \mu\, (\partial U/\partial n)_{w,z} \tag{19}$$

Where A and τ are surface of the rollers and shear stress, respectively.

4.6 Data Transfer from ELEKTRA to CaPS-EM

ELEKTRA solves the 3-D time-varying magnetic field equations. When the time variation is alternating (steady state), all quantities in ELEKTRA are complex phasors and can be expressed in the form

$$X = X_{avg} \cos(\omega t - \Theta). \tag{20}$$

Consequently, after dot or cross products are obtained with these quantities, the computations come out in the form

$$Y = Z \cos(2\omega t - \Psi). \tag{21}$$

To calculate the average values of $\varepsilon_{ijk} J_j B_k$, $E_i E_i$, and $B_j B_j$ per cycle in Eqs. 7, 8, and 9 from the ELEKTRA postprocessor, it is necessary to output the real part (AC time angle = 0°) and imaginary part (AC time angle = 90°) of the quantities in separate tables and average the values in a separate independent code. The computations are evaluated as follows:

Set the AC time angle = 0° and create the table

$$F_{x1} = J_y B_z - J_z B_y \tag{22a}$$

$$F_{y1} = J_z B_x - J_x B_z \tag{22b}$$

$$F_{z1} = J_x B_y - J_y B_x, \tag{22c}$$

$$E_1^2 = E_x^2 + E_y^2 + E_z^2 \tag{22d}$$

$$B_1^2 = B_x^2 + B_y^2 + B_z^2 \tag{22e}$$

Set the AC time angle = 90° and create the table

$$F_{x2} = J_y B_z - J_z B_y \tag{23a}$$

$$F_{y2} = J_z B_x - J_x B_z \tag{23b}$$

$$F_{z2} = J_x B_y - J_y B_x, \tag{23c}$$

$$E_2^2 = E_x^2 + E_y^2 + E_z^2 \tag{23d}$$

$$B_2^2 = B_x^2 + B_y^2 + B_z^2 \tag{23e}$$

Average the values to obtain

$$F_x = (F_{x1} + F_{x2}) / 2 \tag{24a}$$

$$F_y = (F_{y1} + F_{y2}) / 2 \quad (24b)$$

$$F_z = (F_{z1} + F_{z2}) / 2. \quad (24c)$$

$$E_iE_i = (E_1^2 + E_2^2) / 2 \quad (24d)$$

$$B_jB_j = (B_1^2 + B_2^2) / 2 \quad (24e)$$

4.7 Potentials and Boundary Conditions

In ELEKTRA, the choice of potential type in each region depends on the properties of the region. Either reduced potential or total potential can be used in current-free regions, whereas vector potential must be used in eddy-current regions. In this application, reduced potential is used in the air region, total potential is used for the laminated material, and vector potential is applied to liquid Indalloy, copper shield, roller, carbon steel tube, and carbon steel plate.

The boundary conditions of the thermal hydraulics used in this study are symmetry about the center line, no slip at the solid surfaces introduced through wall functions, free surface at the top of the liquid metal, and free surface at the interface between the liquid metal and the air gap. We think that these boundary conditions do not introduce a serious error that will affect the overall system. For isothermal flow of liquid metal, heat transfer will not occur between the liquid Indalloy and the ambient air, and the energy equation is not solved.

5 System Layout

The basic concept for the EMD to provide containment in twin-roll casting is to create a primary time-varying magnetic field that penetrates a passive conductor (the liquid metal to be contained). As the time-varying field changes, an EM force is generated in the plane at right angles to the direction of the changing flux and produces a perpendicular current flow within the liquid metal. The induced current interacts with the primary magnetic field to create a body force (Lorentz force) on the liquid metal that repels the conductor away from the source of the primary field and contains the molten metal. The body force on the liquid metal is the vector cross product of the induced current density and the magnetic flux density. The design problem reduces to that of placing a confinement coil or coils so that a desired free-surface shape can be obtained or metal can be confined against a specified static head.

Figure 6 is schematic representation of one EMD in a static-test-rig configuration, called the proximity type EMD [15,16]. A copper conductor is placed parallel to the plane of the desired containment. A large AC current passes through the conductor and is concentrated on the face of the conductor closest to the liquid metal. Because of the proximity of the conductor to the liquid metal, AC vertical current creates a horizontal magnetic field. The liquid metal that is to be contained interacts with the magnetic field, and the containment forces are generated. These forces support the liquid metal until it passes the kissing point of the rollers. In this design, a high-

permeability laminated material that surrounds the conductor enhances this effect and concentrates the magnetic flux density. The size of the air gap inside the laminated material decreases from bottom (nip) to top and is used to adjust the magnetic field. The copper shield that surrounds the laminated material confines the magnetic field.

A computer model was developed to simulate the schematic representation and three tests were performed to compare model results. In Test 1, a configuration with a static test rig (i.e., rollers do not rotate) was simulated with operating current I = 3.74 kA and frequency f = 4.23 kHz when there is no liquid metal between two rollers. In Test 2, the configuration was the same as in Test 1 but I = 13 kA, f = 4.4 kHz, and liquid Indalloy was placed in front of the magnet (Indalloy has low melting temperature and is used to simulate liquid steel in laboratory tests). In Test 3, a dynamic casting condition was considered. To analyze the containment, computations were made for I = 23.5 kA, f = 1.6 kHz, and liquid steel AISI304. The main parameters of the computational data used in tests are summarized in Table 1.

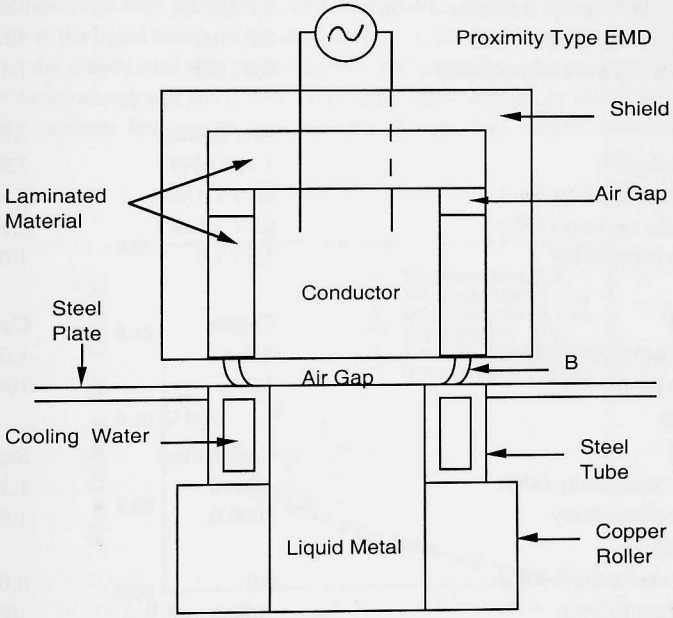

Fig. 6. Schematic representation of EMD in twin-roll casting

Table 1. Parameters of computational setup

Parameter	Test Rig Values Static / Static (Test 1 / Test 2)	Dynamic (Test 3)
Magnetic Coils		
No phases	1 / 1	1
Operating current (kA)	3.74 / 13	23.5
Frequency (kHz)	4.23 / 4.4	1.6
EMD Geometry		
Air gap between EMD and liquid metal (mm)	5.0 / 5.0	5.0
Dimension of twin-roll nip (mm)	10.0 / 10.0	3.0
Diameter of roller (mm)	120.0 / 120.0	120.0
Height of liquid metal containment (mm)	0.0 / 25.0	33.0
Casting speed (m/min)	0.0 / 0.0	40.0
Rotational speed of rollers (rad/s)	0.0 / 0.0	1.112
Liquid Metal		
Material	Air / Indalloy	AISI304
Density (kg/m^3)	1.135 / 8440	7200
Electric conductivity (S/m)	0.0 / 1.41e+6	1.39e+6
Kinematic viscosity (m^2/s)	0.0 / 2.14e-3	2.19e-3
Relative permeability	1.0 / 1.0	1.0
Roller		
Material	Copper	Carbon
Electric conductivity (S/m)	5.0e+7	1.0e+6
Relative permeability	1.0	1000.0
Tube and Plate		
Material	Carbon Steel	Stainless Steel
Electric conductivity (S/m)	1.0e+6	1.39e+6
Relative permeability	1000.0	1.0
Laminated material		
Electric conductivity (S/m)	0.0	0.0
Relative permeability	1000.0	1000.0
Shield		
Material	Copper	Copper
Electric conductivity (S/m)	5.0e+7	5.0e+7
Relative permeability	1.0	1.0

6 Results and Discussion

In Fig. 7, the measured and calculated magnetic flux density (B_x) is shown as a function of the vertical distance at the centerline of a 5-mm air gap when I = 3.742 kA and f = 4.231 kHz for the EMD in a static test rig (Test 1). Also included are data for locations 2 and 4 cm to the left of the centerline when there is no liquid metal (Indalloy) in the containment. The computational results agree well with the measured data along the vertical distance of the air gap.

The stored energy (integral B•H/2 dv) and power loss (integral J**2/σ dv) of the materials used in EMD applications (Test 1) are shown in Table 2. The percentage of each material is the ratio with respect to all of the materials (five materials in this case). From this table, we can see that most of the power is lost in the carbon steel tube (60.6% for stored energy and 94.6% for power loss) because of its high permeability (Table 1). With high-energy consumption and high Joule heating in the carbon steel tube, cooling water is required in the design shown in Fig. 6. However, even with this disadvantage, carbon steel is still used because it can confine the magnetic flux, and because of its high permeability and shallow skin depth, it provides a uniform magnetic field that crosses the liquid metal. Because most of the magnetic flux density is confined within the skin depth of the carbon steel tube, little magnetic flux penetrates into the carbon steel plate and induces low stored energy and power loss. The copper roller and copper shield contain little stored energy and experience little power loss because of their high electric conductivity and low permeability.

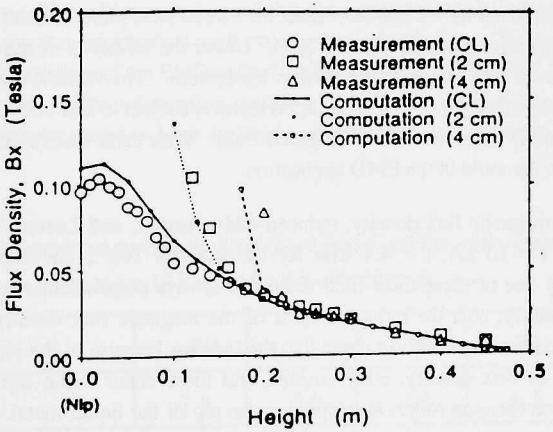

Fig. 7. Measured and calculated magnetic flux density (B_x) as function of vertical distance from nip at centerline of 5-mm air gap for EMD in static test rig (Test 1).

Table 2. Stored energy and power loss in EMD materials

Materials	Stored Energy (%)	Power Loss (%)
Copper Roller	2.7	0.3
Carbon Steel Tube	60.6	94.6
Carbon Steel Plate	2.9	4.8
Laminated Material	32.0	0.0
Copper Shield	1.8	0.3

Figure 8 shows the distribution of the magnetic flux density vector at a cut plane, 15 cm above the nip, of the EMD (I = 13 kA, f = 4.4 kHz) in a twin-roll casting static test rig (Test 2). In this figure, with high permeability in the laminated material and low permeability in the copper shield, magnetic flux concentrates in the laminated material; then crosses the air gap; passes through the skin depths of the carbon steel tube, the carbon steel plate, and the Indalloy; and finally returns to the laminated material in a closed loop. Under the influence of the periodic current, the conductor generates a variable magnetic field in the system. The variable magnetic field, in turn, gives rise to an induced current. Thus, the liquid metal is subject to EM body forces caused by the interaction of the eddy currents and the magnetic field. With these EM forces, liquid metal could be confined within the mold in the EMD application.

Profiles of magnetic flux density, induced eddy current, and Lorentz's force in the liquid metal Indalloy at I = 13 kA, f = 4.4 kHz for the EMD in Test 2 are displayed in Figs. 9a-c, respectively. Any one of these three field vectors is always perpendicular to the others. At the surface of the Indalloy, near the inductor, most of the magnetic flux density, eddy current, and magnetic forces accumulate at a short depth into the Indalloy because of the skin depth effect. The maximum values of flux density, eddy current, and force occur at the nip of the liquid metal because the distance between rollers is minimal at the nip of the liquid metal. Maximum magnetic force is necessary to overcome the maximum hydrostatic pressure at the nip. From the design standpoint, the induced magnetic force must be large enough to overcome the hydrostatic pressure of the liquid metal and to confine the liquid metal inside the container.

Figure 10 presents the free surface profile of the liquid metal Indalloy in a twin-roll casting static test rig with an EMD (I = 13 kA, f = 4.4 kHz, Test 2). The volume fraction method was introduced to track the free interface between the liquid metal and the air gap. The shape of the free surface is governed primarily by the balance of EM pressures against pressures due to gravity. With the capability to predict free-surface shape, the design problem reduces to that of placing a conducting coil or coils so that a desired free surface can be obtained or that metal can be confined against a specified static head.

In Figure 11, the velocity profile of the liquid metal Indalloy is shown under EM fields (I = 13 kA, f = 4.4 kHz) in a static test rig (Test 2). The EM fields and gravity induce the circulation flow pattern, and the velocity is transported inside the liquid metal by fluid viscosity, especially turbulence viscosity. The maximum velocity (4.47 m/s) occurs at the nip of the liquid metal, near the inductor, because of the maximum magnetic force at that location.

Figures 12a and 12b, which show the confinement of the liquid metal Indalloy for operating currents of I = 13 kA, f = 4.4 kHz, and I = 18 kA, f = 4.4 kHz, respectively, in a twin-roll casting static test rig (Test 2), are the free-surface shapes observed from a vertical plane cut through the center of the liquid metal. In Fig. 12a, with I = 13 kA, the top of the pool barely touches the magnet at the locations that are close to the surface of the roller. Here, the top does not mean the height at the liquid metal head, which is 25 cm above the nip, but a height ≈18-22 cm above the nip. In other words, liquid metal may touch the magnet near the roller surface at a height of ≈18-22 cm, and, above 22 cm, it is pushed far away from the magnet. Below 18 cm, liquid metal is well contained. In Fig. 12b, with a stronger current (I = 18 kA) in the coil, liquid metal is contained everywhere. It should be emphasized that the computer model accurately predicts the containment at locations that are identical with experimental observation. The push-back distance of liquid Indalloy from the face of the EMD under EM force is shown in Table 3 for the case when I = 18 kA, f = 4.4 kHz. The information included in Table 3 and Figures 12a and 12b was obtained from the computer model and can be used to optimize the caster design for a commercial device.

Table 3. Computer-modeled push-back distances of liquid Indalloy from magnetic dam face at I = 18 kA and f = 4.4 kHz (Test 2)

Height above nip (cm)	5	10	15	20	25
Push-back (mm)	7.8	7.0	6.5	6.5	27

Profiles of magnetic flux density, induced eddy current, and Lorentz force in the metal AISI304 at I = 23.5 kA and f = 1.6 kHz in a dynamic test rig (Test 3) are presented in Figs. 13a-c,

respectively. Each of these three field vectors is always perpendicular to the others. At the liquid metal surface near the conductor, most of the magnetic flux density, eddy current, and magnetic force accumulate at a shallow depth into the metal because of the skin depth effect. The maximum values of flux density, eddy current, and force occur at the nip of the liquid metal, because the distance between rollers is minimal there.

While Fig. 14a presents the free-surface profile of the liquid metal stainless steel (AISI304) in an operating twin-roll caster (Test 3) with an EMD (I = 23.5 kA, f = 1.6 kHz), Fig. 14b shows the free-surface shapes observed from a vertical plane cut through the center of the liquid metal. With the EMD, liquid metal is contained with a pool height of 33 cm everywhere. The volume fraction method was introduced to track the free interface between the liquid metal and the air gap. The shape of the free surface is governed primarily by the balance of EM pressures against pressures due to gravity, stirring, and metal feeding. Again, with the capability to predict free surface shape, the design problem is reduced to that of placing a conducting coil or coils so that a desired free-surface can be obtained or that metal can be confined against a specified static head.

The velocity profile of the liquid metal AISI304 for an operating twin-roll caster (Test 3) is presented in Fig. 15. EM fields, gravity, and metal feeding induce the circulation flow pattern. Maximum velocity occurs at the nip of the liquid metal, near the conductor, because of the maximum magnetic force at that location.

Table 4 shows computed and measured values of push-back distance at the centerline of the liquid pool (AISI304) from the EMD face when I = 23.5 kA, f = 1.6 kHz. The results show that the calculated push-back distances are slightly shorter than the measured distance, because the experimental data were measured under static conditions and the force caused by metal feeding was not included. The information in Table 4 was obtained from the computer model and can be used to optimize the caster design for a commercial device.

Table 4. Measured and computer-calculated push-back distances (mm)
of liquid stainless steel (AISI304)
from magnetic dam face at I = 23.5 kA and f = 1.6 kHz (Test 3)

Height of liquid metal Above the nip (cm)	at Nip	5	10	15	20	25	30
Measured (Static case)	27.5	26.0	24.5	18.8	17.5	15.0	17.5
Calculated (Dynamic case)	24.7	24.7	24.2	19.3	16.9	15.5	16.9

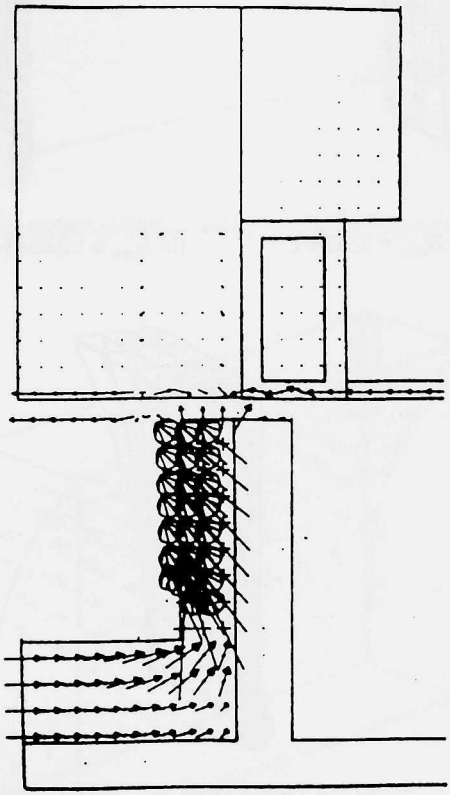

Fig. 8. Distribution of magnetic flux density vector at cut plane of EMD in twin-roll casting

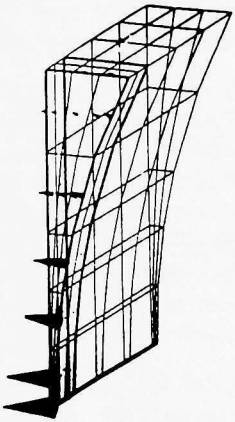

(a) B_{max} = 1.28 T, B_{min} = 5.3E-6 T

(b) J_{max} = 1.22E+8 A/m^2, J_{min} = 5830 A/m^2

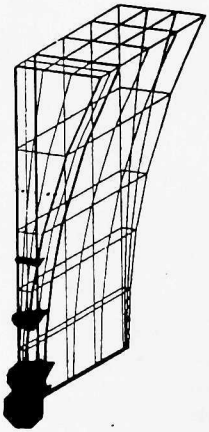

(c) F_{max} = 1.5E+8 nt/m^3, F_{min} = 0.06 nt/m^3

Fig. 9. Field distribution in liquid Indalloy at I = 13 kA, f = 4.4 kHz: (a) magnetic flux density, (b) eddy current, and (c) magnetic force.

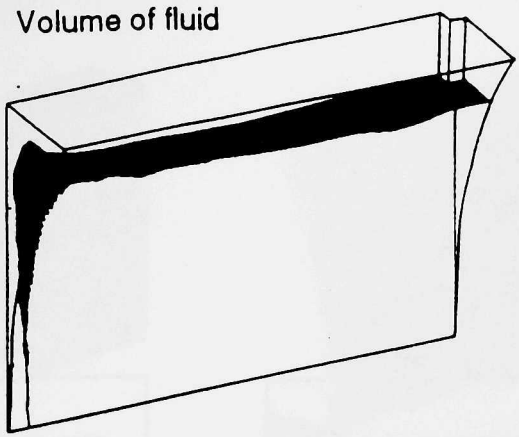

Fig. 10. Free surface of liquid Indalloy in twin-roll casting with EMD

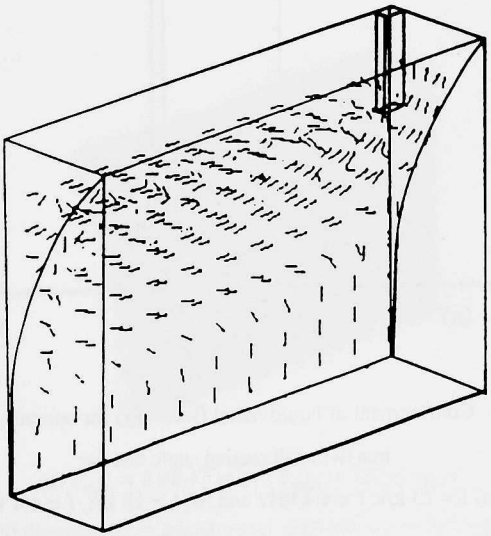

Fig. 11. Velocity profile of liquid Indalloy in twin-roll casting with EMD

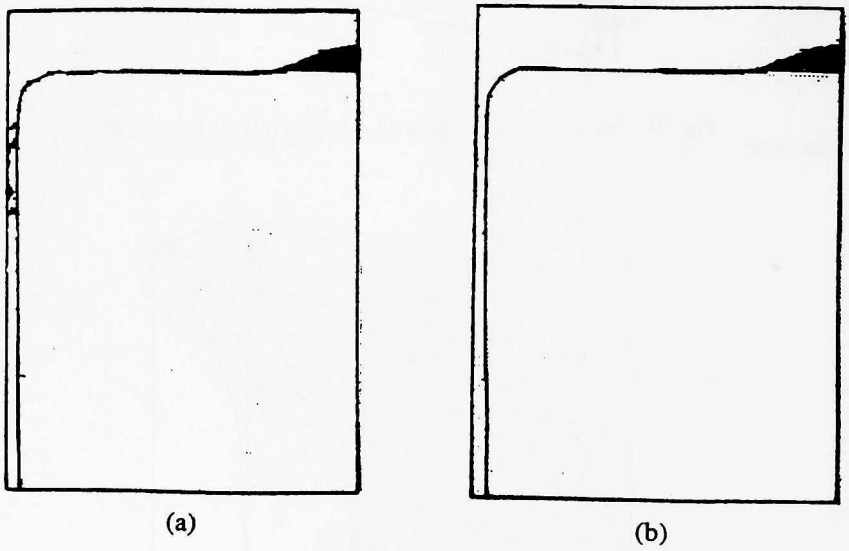

Fig. 12. Confinement of liquid metal (Indalloy) for operating currents in a twin-roll casting static test rig:
(a) I = 13 kA, f = 4.4 kHz and (b) I = 18 kA, f = 4.4 kHz

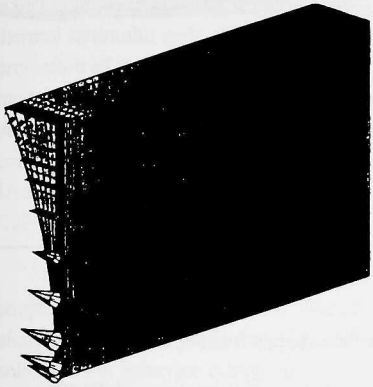

(a) B_{max} = 1.28 T, B_{min} = 5.44E-7 T

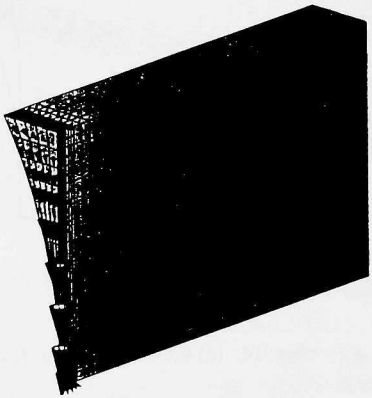

(b) J_{max} = 8.1E+7 A/m^2, J_{min} = 0.2 A/m^2

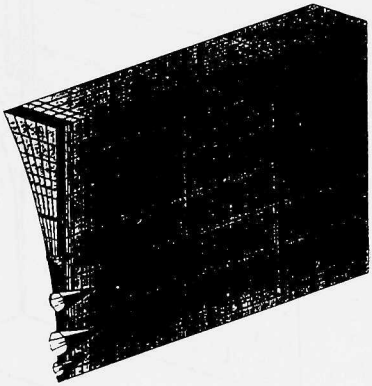

(c) F_{max} = 8.0E+7 nt/m^3, F_{min} = 1.8E-7 nt/m^3

Fig. 13. Field distribution in liquid metal AISI304 at I = 23.5 kA, f = 1.6 kHz: (a) magnetic flux density, (b) eddy current, and (c) magnetic force.

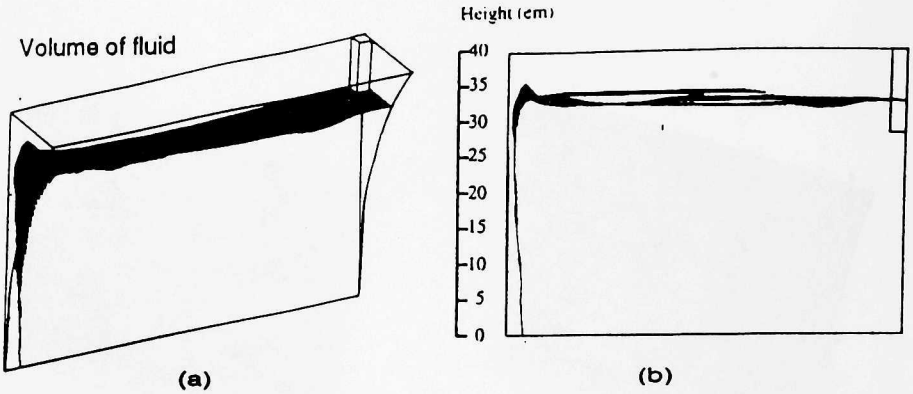

Fig. 14. (a) Free-surface profile and (b) free-surface shapes from vertical plane cut through center of liquid metal AISI304 in dynamic twin-roll casting with EMD

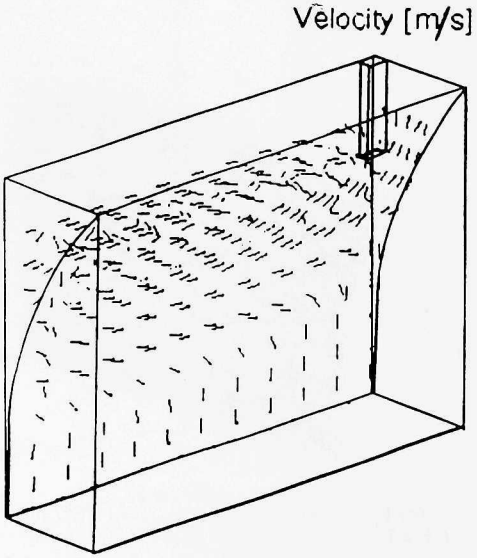

Fig. 15. Velocity profile of liquid metal AISI304 in dynamic twin-roll casting with EMD

7 Summary

Numerical simulations of the EM fields and the fluid flows within liquid metal have been performed for a thin-strip twin-roll casting static test rig with an EMD that closely approximates an actual continuous casting arrangement. The coupling of a 3-D EM code (ELEKTRA) and a 3-D thermal hydraulic code (CaPS-EM) provided encouraging consistency and a reasonably accurate prediction of the flow pattern, free-surface shape, and EMD containment. The developed computer model can predict EM fields, eddy currents, free surface, and fluid flows, and provides a better understanding of EM casters. The model presented here demonstrates the feasibility of full-face containment by the EMD under various operating conditions. The Appendix of this report is a User's Guide for Modeling of MHD Edge Containment in Strip Casting with ELEKTRA and CaPS-EM Codes

The followup work on this research will be the development of a 3-D model for two-way coupled-field analysis that will include the iteration between EM fields and fluid flows. An analysis of heat transfer and induction heat will be required to gain an understanding of solidification behavior during the process. Modeling for surface cracks during solidification of liquid metal in twin-roll casting will be developed to optimize the design of EM twin-roll casters.

Acknowledgments

This work was sponsored by the U.S. Department of Energy, Office of Energy Research under a Cooperative Research and Development Agreement (CRADA) and ISPAT Inland, Inc., formerly Inland Steel Company (WFO Contract). The author expresses his gratitude and thanks for the efforts of Dr. Yeou-Hsin Wang and Dr. Ken Blazek at Inland Steel Research Laboratories. Sincere gratitude and thanks are expressed to Drs. Larry Turner, Hank Domanus and Bob Schmitt, colleagues at ANL, for their guidance and support in using ELEKTRA and CaPS-EM codes in the project. The author expresses thanks to Drs. John Hull and Richard Valentin, ANL, for their support, management, and encouragement throughout.

Appendix

User Guide for
Modeling of MHD Edge Containment in Strip Casting

1 Input and Output Data of ELEKTRA

The ELEKTRA code is commercial software developed by VECTOR FIELDS Inc. (Oxford, England) for 3-D eddy-current computation and electromagnetic (EM) design.

1.1 Material Definition Mode

Material property definitions consist of two compulsory key words and several options that add special properties or control settings of several volumes simultaneously.

The first key word in material definition of ELEKTRA is the "material name." This can be any character string of up to 8 characters, beginning with a letter. There are two predefined material names, AIR and NULL. AIR is for any non-conducting volume with a relative permeability of unity. Volumes with name NULL are omitted from the final mesh, enabling the creation of holes in the mesh to represent, e.g., electrodes. The definition of each material in terms of its permeability and, if necessary, conductivity, is supplied during the commands that create the analysis data file.

The second key word is the "potential type." These are REDUCED, TOTAL, and VECTOR. The following rules must be followed in ELEKTRA. REDUCED scalar potential must be used in a space where source currents are flowing. It is often easiest to make all of the AIR use reduced scalar potential but a model should not have only REDUCED potential volumes.

TOTAL scalar potential can also be used in any AIR volumes. It is also possible to use REDUCED scalar potential but this should only be used as a last resort, if it is not possible to specify a region where the total scalar potential would be single valued. Total scalar potential can also be used in any AIR volumes, which do not contain source currents. This reduces the number of nodes at which the coil field must be calculated and also improves the accuracy of the total field in situations where the fields from the coils and the magnetic materials almost cancel.

Magnetic VECTOR potential must be used in non-AIR volumes with non-zero conductivity. In some situations, it must also be used in adjacent AIR or other non-conducting volumes so that the total magnetic scalar potential in surrounding volumes is single valued. In some models it is convenient to assign a current density to volumes of the mesh. These non-AIR volumes should be modeled with magnetic VECTOR potential and should have zero conductivity.

ELEKTRA can solve problems with constant permeability (linear) or with a defined relationship between flux density and field intensity (nonlinear).

MU	Isotropic permeability
MUXX	X-component of anisotropic permeability

MUYY	Y-component of anisotropic permeability
MUZZ	Z-component of anisotropic permeability
SIGMA	Electrical conductivity
VELX	X-component of velocity
VELY	Y-component of velocity
VELZ	Z-component of velocity
VMOD	Magnitude of velocity: SQRT(VELX**2+VELY**2+VELZ**2)
FREQ	Frequency (steady-state AC)

1.2 Input Parameters of Conductor

The ELEKTRA code contains a wide range of predefined conductor geometries, ranging from simple solenoids to bedsteads and racetracks wound on the surface of cylinders. The code also contain primitive conductor elements that can be joined together to build up conductor circuits. The following conductors are available [19,20]:

- Solenoid around one axis
- Racetrack around one axis
- Bedstead around one axis
- Helical end racetrack
- Circular-arc element
- 8-node brick element
- Generally orientated solenoid
- Generally orientated racetrack
- Generally orientated bedstead
- Constant-perimeter end racetrack
- Straight bar element
- 20-node brick element

To enable conductors to be oriented in space correctly, local coordinate systems can be defined; to reduce the amount of data necessary for symmetry and reflection, the code can be used to replicate a basic shape. In the conductor file, parameters common to all conductors, including the local coordinate systems and replication parameters, will be described first, before details of the conductor shapes are given. Finally, the parameters of the subcommands are listed.

The parameters of subcommands are current density, drive label, and tolerance. The current flowing in the conductors is defined by current density (CURD). For conductors with changing cross section, the current density applies to the first face of the conductor. For time-dependent problems, the PHASE parameter is used to specify a drive label. The SOLVERS command allows each value of the drive label to be associated with a phase angle (steady-state AC) or a drive function (transient).

The fields from some conductors are calculated by an adaptive integration method that requires the user to supply a TOLERANCE that specifies the error tolerance on the flux density in the units that the system is using. The field from conductors without a TOLERANCE parameter, or with TOLERANCE set equal to zero, is calculated to a tolerance of 10 gauss. A negative value

of TOLERANCE can be used to require a single filament approximation to the conductors. The actual value of a negative tolerance is irrelevant.

1.3 Output of Potential and Field Values

POT	Magnetic or electric scalar potential
BX,BY,BZ	Magnetic flux density
BMOD	Magnitude of magnetic flux density: SQRT(BX**2+BY**2+BZ**2)
HX,HY,HZ	Magnetic field strength
HMOD	Magnitude of magnetic field strength: SQRT(HX**2+HY**2+HZ**2)
DX,DY,DZ	Electric flux density
DMOD	Magnitude of electric flux density: SQRT(DX**2+DY**2+DZ**2)
EX,EY,EZ	Electric field strength
EMOD	Magnitude of electric field strength: SQRT(EX**2+EY**2+EZ**2)
JX,JY,JZ	Current density
JMOD	Magnitude of current density: SQRT(JX**2+JY**2+JZ**2)
AX,AY,AZ	Magnetic vector potential
AMOD	Magnitude of magnetic vector potential: SQRT(AX**2+AY**2+AZ**2)
FX,FY,FZ	Force
FMOD	Magnitude of force: SQRT(FX**2+FY**2+FZ**2)
ENERGY	Stored energy
POWER	Power loss

Not all field values apply to all problems, and the precise meaning of the scalar potential depends on the potential type of the element concerned (TOTAL magnetic scalar potential, REDUCED magnetic scalar potential, or electric scalar potential in VECTOR regions or electrostatics problems).

2 Input and Output Data of CaPS-EM

*2.1 *TS Input file Description*

2.1.1 Introduction

When the geometry is set, the initial and boundary conditions for the various sections of the geometry are assigned, and the geometry is meshed; a simulation run can be conducted. The simulation requires input parameters about the extent of the run, time-step size, etc. This input file, the *TS file, is created with the vi editor. The various run-control parameters are described below. Of course, only a few parameters are required but all parameters are included to demonstrate the

vast applications of the CaPS-EM software. The computational domain is partitioned into several computational cells, each bounded by consecutive x- and y-direction grid planes. Surfaces (portions of a plane) may be defined on the exterior, bounding the computational domain, and in the interior. The intersection of a surface and consecutive grid planes outlines a surface element.

User input is read from a file associated with Unit 5 and is called the *TS file, where the * signifies the project name. This input consists of two required namelists. The *BC file, which may contain several other record groups (such as thermal structures), also facilitates in setting up the initial and boundary conditions. The term record corresponds to the earlier concept of a card image. The user may specify Unit 5 or the *TS input file in any order. One possible order is

Problem description and comments (Optional)
Namelist/geom/
Namelist/data/

Below, we describe the variables that may be used in the Namelist/geom/ and Namelist/data/ sections of the TS file. An asterisk in parenthesis (*) indicates that the corresponding value is assigned to the variable as default.

2.1.2 Namelist/geom/

iemf — Flag to include electromagnetic field calculations,
= 1 Calculations of electromagnetic fields.

ifvof — Flag to enable volume of fluid calculations,
= 1 Calculations of volume of fluid.

iroll — Flag to enable dynamic rollers
= 0 Static test rigs (non-rotating rollers),
= 1 Dynamic test rigs (rollers rotating around X-axis),
= 2 Dynamic test rigs (rollers rotating around Y-axis),
= 3 Dynamic test rigs (rollers rotating around Z-axis).

isolve — Flag to determine the solution technique used to solve the energy equations,
= 0 Successive overrelaxation (SOR) solution scheme is used.

isolvr — Flag to determine the solution technique used to solve the pressure equations,
= 0 Successive overrelaxation (SOR) solution scheme is used,
= 11 Preconditioned conjugate gradient solver is used.

iturke — Flag to enable turbulence flow model,
= 0 No-turbulence model,
= 12 k-ε two-equation turbulence model is used.

2.1.3 namelist/data/

alpha	= 0.0	Semi-implicit time advancement for momentum and energy equations,
	= 1.0	Fully implicit time advancement for momentum and energy equations (*).
ifmom	= 0	No momentum calculation,
	= 1	Momentum calculation is performed (*).
ifener	= 0	No energy calculation,
	= 1	Energy calculation is performed (*).
istate	= 2	Beginning of a transient run (*),
	= 3	Continuation of a transient run.

Time- and Time-Step-Related Parameters

dt(1)		Initial time-step size, second.
dt(2)		Maximum time-step size, second. This value is used when automatic time Step is enabled, **idtime = 1**.
idtime	= 0	Time-step size is taken from the user-specified variable dt.
	= 1	Time-step size is computed internally as the product of the largest allowable time increment given the conditions (Courant time-step size and a user-specified variable, **rdtime**).
ntmax		Maximum time-step number for this run. Normal termination occurs after completion of this time step (99999).
rdtime		Time-step size is computed internally as the product of the largest allowable time increment, given the conditions. This value is used only if **idtime = 1**.
timax		Maximum time of this run. Normal termination occurs after this time has been reached, second (3.6E+7). timax refers to the simulation or problem time, not the computer CPU time needed to run the problem.
tstart		Initial time, second (0.0). This value should be reset to zero at the beginning of a transient run, **istate = 2**.
ntplot		Up to 25 values to specify when step information is to be written. The following are acceptable values of **ntplot**:
	= 0	No more step information is written (*).
	> 0	Time-step number for which step information is written. After the nth positive time step in **ntplot** has been processed, the (n+1)th value of **ntplot** is used to determine which subsequent time steps are written to the RUN directory.
	< 0	A value -n indicates that information is written to the RUN directory every nth time step. No subsequent values of **ntplot** are considered. Example: **ntplot**

= -5 indicates that every fifth step is to be processed. **ntplot** = 5, 10 -20 indicates that steps 5, 10, 20, 40, 60, etc., are to be processed. **ntplot** = 10, 20, 0 indicates that only steps 10 and 20 are to be processed.

Iteration Control Parameters

eps1	Mass convergence criterion parameter (1.0E-4).
eps2	Mass convergence criterion parameter (1.0E-6).
eps3	Implicit convergence criterion parameter (5.0E-5).
eps5	Energy solver convergence criterion parameter (1.0E-5).
it(1)	Number of iterations permitted for time steps.
itmaxp	Number of iterations in the pressure solver (99).
itmaxe	Number of iterations in the energy solver (99).
omega	Relaxation factor for the SOR pressure solver (1.5).
omegad	Underrelaxation factor for the turbulence kinetic energy dissipation coefficients (0.7).
omegae	Underrelaxation factor for the energy equation coefficients (1.0).
omegak	Underrelaxation factor for the turbulence kinetic energy coefficients (0.7).
omegav	Underrelaxation factor for the momentum equation coefficients (1.0).
relaxe	Relaxation factor for the SOR energy solver (0.95).
gravx	X-component of gravity vector, m/s^2 (0.0).
gravy	Y-component of gravity vector, m/s^2 (0.0).
gravz	Z-component of gravity vector, m/s^2 (0.0).
pvoid	Back-pressure exerted on the free surface.

Electromagnetic-Field Control Parameters

icase	= 0	No cell output data for EMD applications (*).
	= 1	Cell output data for EMD applications.
ifreq		Electromagnetic data input flag
	= 1	Input the data of EM fields and eddy currents from ELEKTRA to CaPS-EM.
	= 2	Input the data of EM fields and EM forces from ELEKTRA to CaPS-EM (*).
cele		Electric conductivity (0.0).
cmhd		Magnetic-effect constant (0.1).

clock	Time with constant voltage (0.0).
bmod1	Coefficient 1 for modified magnetic/electric field (0.0).
bmod2	Coefficient 2 for modified magnetic/electric field (0.0).
bmod3	Coefficient 3 for modified magnetic/electric field (0.0).
bmod4	Coefficient 4 for modified magnetic/electric field (0.0).
bmod5	Coefficient 5 for modified magnetic/electric field (0.0).
bmod6	Coefficient 6 for modified magnetic field (0.0).
bmod7	Coefficient 7 for modified magnetic field (0.0).
bmod8	Coefficient 8 for modified magnetic field (0.0).
fmod1	Coefficient 1 for modified EM force/factor (0.0).
fmod2	Coefficient 2 for modified EM force/factor (0.0).
fmod3	Coefficient 3 for modified EM force/factor (0.0).
fmod4	Coefficient 4 for modified EM force/factor (0.0).
fmod5	Coefficient 5 for modified EM force/factor (0.0).
fmod6	Coefficient 6 for modified EM force (0.0).
fmod7	Coefficient 7 for modified EM force (0.0).
fmod8	Coefficient 8 for modified EM force (0.0).
cofemf	Adjustment coefficient of magnetic effect (1.0).

Dynamic Roller Control Parameters

nmr	Number of cells with wall shear force.
angvel	Angular velocity of roller, rad/s (0.0).
coroll	Adjustment coefficient of roller wall friction (1.0).
droll1	Starting length of rollers (0.0).
droll2	Ending length of rollers (0.0).
hmetal	Height of liquid metal (0.0).
radius	Radius of twin rolls (0.0).
xcroll	X coordinate of roller center (0.0).
ycroll	Y coordinate of roller center (0.0).
zcroll	Z coordinate of roller center (0.0).

2.2 Print Step

2.2.1 Introduction

A hard-copy output of the various variables can be obtained by creating a *.PS file in the current working-run directory. This file directs CaPS-EM as to which variables are to be printed and can be initiated after any of the evolved step files, which are the binary simulation result files. As an example, this file appears as

K - plane 3
Variables ul p tl bemf cemf femf

Where the plane of interest is the kth-plane, clipped 3 cells in the z-direction. Multiple planes can also be printed by writing the plane of interest in the *.PS file.

2.2.2 Description of Cell Output Variables

ul	X-component of velocity (m/s)
vl	Y-component of velocity (m/s)
wl	Z-component of velocity (m/s)
hl	Enthalpy (J/kg)
tl	Temperature (Celsius)
al	Volume porosity
rl	Density (kg/m3)
P	Pressure (Pa)
tk	Turbulence kinetic energy (J/kg)
qsour	Volumetric heat source (w/m^3)
rmu	Molecular viscosity (Pa*s)
turcon	Turbulent conductivity [W/(m*K)]
turvis	Turbulent viscosity (Pa*s)
rcon	Molecular conductivity [W/(m*K)]
xms	Solid mass fraction
vfluid	Cell fluid volume (m^3)
vof	Volume of fluid
td	Dissipation of turbulence kinetic energy (W/kg)
spheat	Specific heat [J/(kg*K)]
eke	Flow kinetic energy (J/kg)
bemfx	X-component of magnetic flux density (Tesla)
bemfy	Y-component of magnetic flux density (Tesla)

bemfz	Z-component of magnetic flux density (Tesla)
bemf	Magnetic flux density (Tesla)
cemfx	X-component of current density (A/m^2)
cemfy	Y-component of current density (A/m^2)
cemfz	Z-component of current density (A/m^2)
cemf	Current density (A/m^2)
eemfx	X-component of electric potential (Volt/m)
eemfy	Y-component of electric potential (Volt/m)
eemfz	Z-component of electric potential (Volt/m)
eemf	Electric potential (Volt/m)
femfx	X-component of electromagnetic force (nt/m^3)
femfy	Y-component of electromagnetic force (nt/m^3)
femfz	Z-component of electromagnetic force (nt/m^3)
femf	Electromagnetic force (nt/m^3)
pmag	Average magnetic pressure (Pa)
pfest	Ferrostatic pressure (Pa)
qemf	Resistivity heat (J/m^3)
uroll	X-component of velocity induced by shear force of rotating roller (m/s)
vroll	Y-component of velocity induced by shear force of rotating roller (m/s)
wroll	Z-component of velocity induced by shear force of rotating roller (m/s)

3 Material Properties of CaPS-EM

3.1 Introduction

Material properties are permitted to be temperature dependent in CaPS-EM. Four material-property variables are required: thermal conductivity, density, specific heat, and viscosity. If temperature-dependent properties are available, CaPS-EM linearly interpolates the adjacent properties to provide properties over the entire temperature range, and uses the more elaborate table. Beyond the last property value, CaPS-EM assumes a constant equal to the last property value.

The advantage of using temperature-dependent properties rather than constants is that by doing so, the actual phase change at a particular temperature can be realized. Also, the temperature dependence corresponds to real-world properties, because properties vary as a function of temperature. If only constant properties are available for the particular material, e.g., the solid and liquid state properties, CaPS-EM linearly interpolates the end points and assumes constant values

beyond the table entries. In Section 3.2, we explain how to create a *.prop file in the properties subdirectory.

3.2 Property Database Organization

The properties directory contains the files that defines the properties for all of the materials that are to be available to the CaPS-EM software. The CaPS-EM materials are organized in a library directory, where there exists a file called "available_materials", which is a table of contents of the materials in the library. The properties of a material are in files named "*.prop". The property data are in tabular format, and property data file names are listed in the file. The properties directory already contains several sample properties files. The file name must be no more than 11 alphanumeric characters long, and including the ".prop" extension, it must not be more than 16 alphanumeric characters long.

As mentioned earlier, properties are evaluated by linear interpolation of two adjacent tabular data at the corresponding temperatures. The property value beyond the one that is last defined is considered a constant, with a value equal to the last defined value. Each material file must contain tables for the following properties:

Property	Name	Units
Thermal Conductivity	KXX	(heat*length)/(time*area*temp)
Mass Density	DENS	mass/volume
Specific Heat	C	heat/(mass*temp)
Viscosity	VISC	(force*time)/length2

The state of the casting material can be solid, mushy, or liquid, where mushy is the term used when solid and liquid states coexist. In the mushy case, the solidus and liquidus temperatures also must be specified in the material property database file.

The following is a sample file for the stainless steel AISI304. This file will be used to explain the various terms.

```
/COM AISI304 (stainless steel)
/COM Electromagnetic Edge Dam
/COM t_liquidus = 1454.0, t_solidus = 1400.0
MPTEMP
MPTEMP,      1,              507.0,    1400.0,    1454.0,    1494.0,
MPDATA,KXX ,  1,   1,         22.4,      34.1,      28.1,      28.6,
MPTEMP
MPTEMP,      1,              1400.0,    1454.0,
MPDATA,DENS,  1,   1,        7900.0,    7200.0,
```

```
MPDATA,VISC,    1,   1,   1.00e00,  2.193E-3,
MPTEMP
MPTEMP,         1,              507.0,   1400.0,   1400.0,   1454.0,   1454.0,   1494.0,
MPTEMP,C        ,   1,   1,   598.1,    684.9,    6057.3,   6057.3,    689.0,    692.1,
```

The following aspects of the above files must be noted:

/COM — Comment lines used to either write references, citations, t_liquidus and t_solidus values, or to_si conversions. The first two lines are read by the Vbounds module of CaPS-EM, which assigns initial and boundary conditions to various parts of the geometry. Thus, the first /COM line must contain the name of the material, and the following line may contain a brief description of the material.

MPTEMP — These are the temperature-specified lines, which may contain, at most, five temperature values per line. The first four spaces after "MPTEMP" are to be used for the index of the following temperature value. Thus, " 1," implies that the temperature value following the comma is the first temperature value, " 6," implies that the following temperature value is the sixth value, and so on.

MPDATA — This is the prompt to define material-property values. Following "MPDATA," either of the properties may be specified, limiting the variable name to four characters. Thus, KXX is the thermal conductivity, DENS is the density, C is the specific heat, and VISC is the viscosity. If the variable name is less than four characters, blank spaces must be specified until four spaces are utilized, followed by a comma. Thus, following "MPDATA,", we can have "KXX ,", "DENS,", "VISC,", or "C ,". The following three spaces are reserved for indexing. This is followed by a comma. The next three spaces indicate the index of the first data value on that line. Thus " 1," indicates that the first data value on that line is the first in the series, " 6," indicates that it is sixth in the series, and so on.

Note that the "to_si" unit conversions can be embedded within each definition of the material properties. In the above examples, the units are all in SI and therefore, "to_si" parameters need not be used. The t_liquidus and t_solidus values follow the comment lines.

Thus, new materials may be made available to CaPS-EM merely by adding a new property file into the materials property database file. After a new material file has been created, the "available materials" file must include the name of the new file for CaPS-EM to identify it. This

can be done by executing the script "make table," which searches for all the *.prop files and appends their names into the "available materials" file.

References

1. Miyazawa, K., and Szekely, J., A Mathematical Model of the Splat Cooling Process Using the Twin-Roll Technique, Metallurgical Transactions A, Vol. 12A(6), 1981, pp. 1047-1057.

2. Saitoh, T., et al., Two-Dimensional Model for Twin-Roll Continuous Casting, Metallurgical Transactions B, Vol. 20B(6), 1989, pp. 381-390.

3. Fujita, Y., et al., Solidification and Roll-Bonding of Shells in Twin-Roll Casting Process, Iron and Steel Institute of Japan International, Vol. 29(6), 1989, pp. 495-502.

4. Shiomi, M., Mori, K., and Osakada, K., Finite Element and Physical Simulations of Non-Steady State Metal Flow and Temperature Distribution in Twin Roll Strip Casting, Modeling of Casting, Welding, and Advanced Solidification Processes Proceedings, Vol. 7, 1995, pp. 793-800.

5. Yukumoto, M., and Yamane, H., Thin Strip Casting of Ni-Base Alloys by Twin Roll Process, 78th Steelmaking Conf. Proc., Vol. 78, 1995, pp. 19-22.

6. Getselev, Z. N., Method of Forming Ingot in a Process of Continuous and Semi-Continuous Casting of Metals, U.S. Patent 4014379, March 29, 1977.

7. Olson, E. A., Method and Apparatus for Excluding Molten Metal from Escaping from or Penetrating into Openings or Cavities, U.S. Patent 4020890, May 3, 1977.

8. Lewis, B. G., Electromagnetic Shaping of Thin Semiconductor Ribbon Strip Cast onto a Chilled Block, U.S. Patent 4562878, Jan. 7, 1986.

9. Lowry, H. R., et al., Continuous Metal Casting Apparatus, U.S. Patent 4662431, May 5, 1987.

10. Tacke, K. H., and Schwerdtfeger, K., Stirring Velocities in Continuously Cast Round Billets as Induced by Rotating Electromagnetic Fields, Stahl & Eisen, Vol. 99(1), 1979, pp. 7-12.

11. Spitzer, K. H., Dubke, M., and Schwerdtfeger, K., Rotational Electromagnetic Stirring in Continuous Casting of Round Strands, Metallurgical Transactions, Vol. 17B, 1986, pp. 119-131.

12. Partinen, J. K., Saluja, N., Szekely, J., and Kirtley, J., Experimental and Computational Investigation of Rotary Electromagnetic Stirring in a Woods Metal System, ISIJ Int'l, Vol. 34(9), 1994, pp. 707-714.

13. Beitelman, L. and Mulcahy, J. A., Flow Control in the Meniscus of Continuous Casting Mold

with an Auxiliary A.C. Magnetic Fields, Int'l Symposium on Electromagnetic Processing of Materials, EPM'94, Nagoya, Japan, 1994, The Iron and Steel Institute of Japan, pp. 235-241.

14. Chang, F. C., Hull, J. R., and Beitelman, L., Simulation of Fluid Flow Induced by Opposing AC Magnetic Fields in a Continuous Casting Mold, 13th Process Technology Conference Proceedings, Iron and Steel Society, Vol. 13, 1995, pp. 79-88.

15. Saucedo, I. G., and Blazek, K. E., Development of an Electromagnetic Edge Dam (EMD) for Twin Roll Casting, METEC-94, pp. 457-462.

16. Blazek, K. E., Gerber, H. G., and Saucedo, I. G., Application of Alternating Magnetic Fields for Edge Containment in Strip Casting, Int'l Symposium on Electromagnetic Processing of Materials, EPM'94, Nagoya, Japan, 1994, The Iron and Steel Institute of Japan, pp. 197-202.

17. Domanus, H. M., Schmitt, R. C., and Ahuja, S., User's Guide for the Casting Process Simulator Software CaPS-2D, Version 1.0, Argonne National Laboratory Report ANL-93/14, July 1993.

18. Trowbridge, C. W., An Introduction to Computer Aided Electromagnetic Analysis, published Vector Fields Ltd., Oxford, England, 1990.

19. OPERA-3D Reference Manual - Software for Electromagnetic Design, published by Vector Fields Ltd., Oxford, England, 1998.

20. OPERA-3D User Guide - Software for Electromagnetic Design, published by Vector Fields Ltd., Oxford, England, 1998.

21. Bird, R. B., Stewart, W. E., and Lightfoot, E. N., Transport Phenomena, John Wiley & Sons, Inc., New York, 1966.

22. Tallback, G., Kollberg, S., and Hackl, H., Simulations of EMBR Influence on Fluid Flow in Slabs, 17th Advanced Technology Symposium, Phoenix, Feb. 13-16, 1994.

23. Chang, F. C., Bottoni, M., and Sha, W. T., Development and Validation of the k-ε Two-Equation Turbulence Model and the Six-Equation Anisotropic Turbulence Model in the COMMIX-1C/ATM, Argonne National Laboratory Report ANL/ATHRP -44, Jan. 1992.

Distribution for ANL-00/1

Internal:

F. C. Chang (5)
T. H. Chien
H. M. Domanus
H. Drucker
A. M. Hassanein
J. R. Hull
C. A. Malefyt
R. B. Poeppel
R. C. Schmitt
L. R. Turner
R. A. Valentin
ANL Patent Dept.
ANL Contract File
TIS Files

External:

DOE-OSTI (2)
DOE Office of Energy Research
ANL Libraries
    ANL-E
    ANL-W
ISPAT Inland, Inc.
    Research Laboratories
        K. Blazek
        Y.-H. Wang
Energy Technology Division Review Committee:
    H. K. Birnbaum, University of Illinois, at Urbana-Champaign, IL
    I.-W. Chen, University of Pennsylvania
    E. M. Logothetis, Ford Motor Co., Dearborn, MI
    H. S. Rosenbaum, Fremont, CA
    S. L. Sass, Cornell University
    R. K. Shah, General Motors Corp., Lockport, NY
    S. Smialowska, Ohio State University, Columbus, OH